

Whence particle acceleration

Mikhail V. Medvedev^a, Anatoly Spitkovsky^b

^a*Dept. of Physics and Astronomy, University of Kansas, Lawrence, KS 66045*

^b*Dept. of Astrophysical Sciences, Princeton University, Princeton, NJ 08544*

Abstract

We discuss how the electrons in relativistic GRB shocks can reach near-equipartition in energy with the protons. We emphasize the non-Fermi origin of such acceleration. We argue that the dynamics of the electrons in the foreshock region and at the shock front plays an important role. We also demonstrate that PIC simulations can directly probe this physics in the regimes relevant to GRBs.

Key words: acceleration of particles, shock waves, gamma-rays: bursts

PACS: 98.70.Rz, 98.70.Qy, 52.35.Tc

Electron acceleration/heating — There is a lore that charged particles are accelerated at shocks by the Fermi mechanism. Numerical simulations show that although Fermi acceleration may be present, it cannot heat the bulk electrons to near-equipartition with the protons, i.e. $\epsilon_e \lesssim 1$. We suggest alternative mechanisms that may be at work in relativistic collisionless shocks.

Magnetic fields are generated at shocks by the Weibel instability (Medvedev & Loeb, 1999; Chang et al., 2007), that saturates its linear phase at a relatively low magnetic field, near the equipartition with the electrons. At such low fields, protons keep streaming in current filaments, whereas the electrons, being much lighter than the protons, are quickly isotropized in the random fields and form a uniform background. Nonlinear evolution of the filaments leads to further amplification of the magnetic field up to $\epsilon_B \sim 0.1$ on average (and $\epsilon_B \sim 1$ locally in clumps) as one approaches the main shock compression. The average Lorentz factor of the electrons is also gradually increasing toward the shock and ϵ_e becomes 30% to 50% around and after the shock jump (Chang et al., 2007; Spitkovsky, in prep.). This electron heating we are trying to understand.

Electrostatic model — The current filaments are formed by the protons moving roughly at the speed of light (their Lorentz factor is $\sim \Gamma$). Hence, they are the sources of both the magnetic and electrostatic fields. In the absence of strong

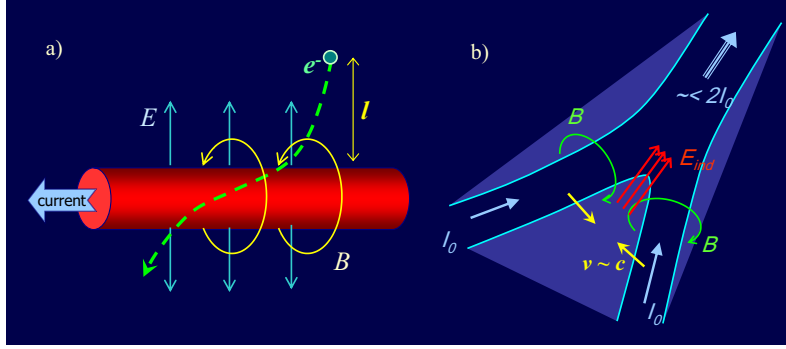


Fig. 1. Acceleration mechanisms. (a) — the electrostatic model, (b) — the filament merger as an example of the induction model.

electrostatic shielding (simulations seem to show this) E and B fields are related as $B \lesssim E$. An electron, moving toward a filament, see Fig. 1a, gains energy $u_e \simeq eEl \simeq eBl$, where l is the radial distance the electron travels through the strong E field region. We normalize it to the characteristic scale in the system, c/ω_{pp} (the typical size of the filaments is few c/ω_{pp}) as $l \simeq \lambda(c/\omega_{pp})$, where $\omega_{pp} = (4\pi e^2 n/m_p \gamma_p)^{1/2}$ is the relativistic proton plasma frequency and $\gamma_p \simeq \Gamma$. The parameter λ accounts for the actual geometry of the filaments, the electrostatic shielding in plasmas, the effects of the electrons on the current distribution, etc. If most of the electrons reside near the filaments (as simulations also seem to show), the electron energy density is estimated as $U_e = nu_e \simeq neB\lambda c/\omega_{pp}$, or in dimensionless units: $\epsilon_e \simeq \lambda\sqrt{\epsilon_B}$. Although this mechanism does not provide the net acceleration (the fields considered are potential), the electrons gain energy locally, and can radiate it away if the cooling timescale in filaments is short enough, see below.

Induction model — The current filaments exhibit violent dynamics in which the field configuration can change rapidly; these include the filament multiple mergers (in the foreshock) and break-up (mostly at the shock jump). Let's consider a merger as an example, Fig. 1b. Two filaments with the typical magnetic field B approaching each other with a velocity, $v \sim c$, induce the non-potential electric field E_{ind} in-between. The typical size of the region with this field is of order the filament size, hence it is $d \sim \delta(c/\omega_{pp})$, where δ is a dimensionless size of the merger region. An electron traversing the region gains energy $u_e \sim eE_{\text{ind}}d \sim e(v/c)B\delta c/\omega_{pp}$. The corresponding electron energy density is $u_e n$. Thus, we obtain $\epsilon_e \simeq (v/c)\delta\sqrt{\epsilon_B}$, which recovers the previous result once λ is replaced with $(v/c)\delta$. Perhaps not all plasma goes through such regions, so this mechanism may explain acceleration of a smaller number of energetic electrons from the tail of the distribution. Unlike the electrostatic acceleration, the inductive acceleration is “permanent”, meaning that the electrons remain energetic in the downstream, where the current filaments are essentially gone.

Relevance to GRBs — The radiative efficiency of a shock is determined by how fast the bulk electrons lose their energy via radiation. If the electron

synchrotron cooling time is smaller than or comparable to the electron residence time in the high field region (near the shock front), this electron will radiate away energy comparable to its kinetic energy. The shock will be radiatively efficient in this regime regardless of the field dynamics in the far downstream. The dimensionless cooling time is defined as $T_{\text{cool}} = t_{\text{cool}}\omega_{pp} = \left(\frac{6\pi m_e c}{\sigma_T \gamma_e B^2}\right) \left(\frac{4\pi e^2 n'}{\Gamma m_p}\right)^{1/2}$, where t_{cool} is the synchrotron cooling time, n' is the particle density behind the shock measured in the downstream frame, Γ is the shock Lorentz factor. The region of strong magnetic field at the shock front, where $\epsilon_B \sim 0.1 - 0.05$ is of the size $d_B \sim 50c/\omega_{pp}$ or so. Since the shock moves at $v = c/3$ in the downstream frame, the residence time in the region of high field is $t_{\text{res}} \sim d_B/v \sim (150 - 300)\omega_{pp}^{-1}$. This estimate, does not account for the filling factor of magnetic inhomogeneities, which shortens the effective t_{res} , and the electron trapping in high-field clumps, which is increasing t_{res} .

If $t_{\text{cool}} \lesssim t_{\text{res}}$, then the electrons lose their energy quickly near the shock jump, hence the radiative efficiency is high and such a shock can be seen as a GRB. We refer to a shock as the “*radiative shock*” if $T_{\text{cool}} \lesssim 300$ and as the “*weakly radiative shock*” otherwise (its efficiency depends on the fields in the far downstream, which have not yet been adequately probed in PIC simulations). In an extreme case, $T_{\text{cool}} < 1$, called the “*radiative foreshock*” regime, radiative cooling will be substantial even before the main shock compression, hence cooling may change the entire shock structure.

Using the standard shock model (Rees & Mészáros, 2005), the comoving density behind an internal shock at a radial distance R from the central engine is $n = 4\Gamma_i L / (4\pi R^2 \Gamma^2 m_p c^3)$, where L is the kinetic luminosity, Γ_i is Γ of an internal shock. The magnetic field and the electron bulk Lorentz factor are fractions ϵ_B and ϵ_e of the post-shock thermal energy density $B' = (8\pi\Gamma_i m_p c^2 n' \epsilon_B)^{1/2}$, $\gamma_e = (m_p/m_e)\Gamma_i \epsilon_e$. Parameters ϵ_B and ϵ_e are $\sim 10\%$ and $\sim 50\%$ as follows from simulations. Finally, the dimensionless cooling time in baryon-dominated internal shocks becomes $T_{\text{cool}}^{(e^-p)} \simeq 170 L_{52}^{-1/2} \Gamma_2 \Gamma_i^{-3} R_{12} \epsilon_B^{-1} \epsilon_e^{-1}$. Similarly, we evaluate the cooling time for the external (afterglow) shocks for the constant density ISM and the Wind ($n \propto R^{-2}$) outflow models (Granot et al., 1999; Chevalier & Li, 2000); the details are in (Medvedev & Spitkovsky, in preparation).

The results are shown in Fig. 2. One can see that internal shocks ($\Gamma_i \sim 4$) with strong foreshock emission, $T_{\text{cool}} \lesssim 1$, can occur for $\Gamma \lesssim 60$ and at $R \lesssim \text{few} \times 10^{10} - 10^{11}$, well below the photosphere at such low Γ 's. Strongly radiative shocks $T_{\text{cool}} \sim 100 - 300$ can occur above the baryonic photosphere in a relatively narrow, but very natural range of parameters, $\Gamma \sim 150 - 400$, $\Gamma_i \gtrsim 2.5$, $R_i \sim 10^{12 \pm 0.5} \text{cm}$ and the outflow kinetic luminosity $L \sim 10^{52 \pm 2} \text{erg/s}$; hence they are likely observable. Since $T_{\text{cool}} \propto \Gamma_i^{-3}$, the region of the parameters widens greatly with increasing Γ_i .

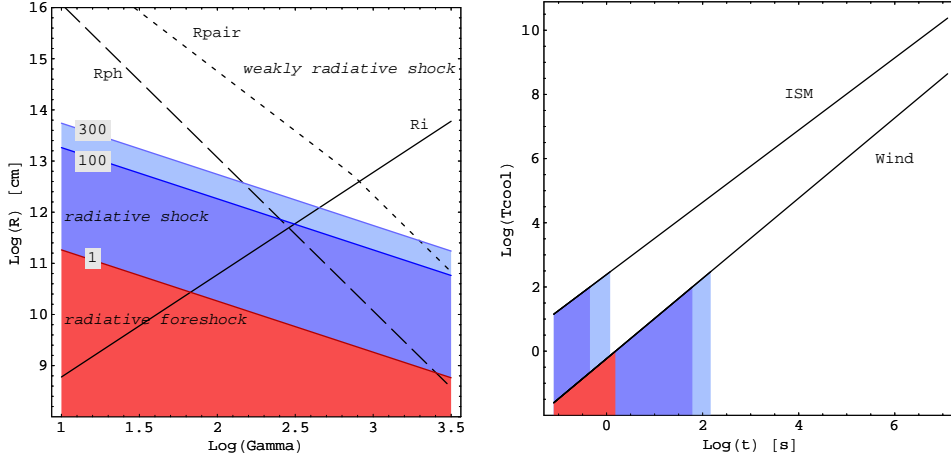


Fig. 2. (*left*) — Contours of T_{cool} vs. Γ for the internal shocks for $T_{\text{cool}} = 1, 100, 300$. Red filled regions correspond to $T_{\text{cool}} < 1$ (radiative foreshock), dark and light blue regions correspond to $1 < T_{\text{cool}} < 100$ and $100 < T_{\text{cool}} < 300$, respectively (radiative shock), and the white region corresponds to $T_{\text{cool}} > 300$ (weakly radiative shock). Here $\Gamma_i = 4$, $L_{52} = 1$, $L_\gamma = 0.1L$, $t_{v,-4} = 1$. We also mark the radii beyond which the internal shocks can form (R_i), the medium is optically thin to Thompson scattering (R_{ph}) and the optical depth due to e^\pm -pairs is below unity (R_{pair}). (*right*) — Cooling time in afterglows vs. time after the burst, for the ISM and Wind models. We use, $E = 10^{54}$ erg, $A_* = 10$ and $n_{\text{ISM}} = 100 \text{ cm}^{-3}$ and a typical $z = 2$.

For external shocks, we also see that, except for the very early times, the afterglow emission should be coming from far downstream, not from the main shock compression region. However, in the Wind model, the external shock can be radiative up to ~ 100 s after the burst, whereas for the ISM model, the radiative shock regime can occur only at times earlier than a second after the explosion. Since the afterglow usually sets in at least several tens of seconds after the explosion (when enough external gas is swept by the shock), we conclude that very early afterglow emission can, in principle, come from radiative shocks propagating in relatively strong Wolf-Rayet winds ($A_* \gtrsim \text{few}$).

It is remarkable that under these conditions, all the emission shall come from a thin shell of thickness $\sim t_{\text{cool}}c \sim 1$ meter (internal shocks) and ~ 100 km (external shocks), that is, from the region of main shock compression. This region is already well resolved in 2D PIC simulations. Moreover, one can obtain the emitted radiation directly from PIC simulations.

References

- Chang, P., Spitkovsky, A., Arons, J. 2007, ApJ, submitted, arXiv:0704.3832
Chevalier, R. A., & Li, Z.-Y. 2000, ApJ, 536, 195
Granot, J., Piran, T., & Sari, R. 1999, ApJ, 527, 236
Medvedev, M. V., & Loeb, A. 1999, ApJ, 526, 697

Rees, M. J., & Mészáros, P. 2005, *ApJ*, 628, 847